

Determination of the dynamical structure of galaxies using optical spectra

S. De Rijcke [★] and H. Dejonghe

*Sterrenkundig Observatorium, University of Ghent,
Krijgslaan 281, S9, 9000 Gent, Belgium*

11 October 2018

ABSTRACT

Galaxy spectra are a rich source of kinematical information since the shapes of the absorption lines reflect the movement of stars along the line-of-sight. We present a technique to directly build a dynamical model for a galaxy by fitting model spectra, calculated from a dynamical model, to the observed galaxy spectra. Using synthetic spectra from a known galaxy model we demonstrate that this technique indeed recovers the essential dynamical characteristics of the galaxy model. Moreover, the method allows a statistically meaningful error analysis on the resulting dynamical quantities.

Key words: Galaxies: kinematics and dynamics–Celestial mechanics, stellar dynamics

1 INTRODUCTION

The construction of a dynamical model for a galaxy depends on two kinds of data. The photometric measurements yield, after deprojection, the mass density. Assuming a mass-luminosity ratio, the Poisson equation then leads to the gravitational potential. The kinematics are obtained by analysing spectral information, with the aim to characterise the line-of-sight velocity distribution (hereafter LOSVD) $\phi(v_p, x_p, y_p)$, which is the probability of finding a star with projected velocity v_p at a position (x_p, y_p) on the sky.

When the signal to noise ratio (S/N) of the data is rather low, a LOSVD can be parametrised as a simple Gaussian. There exist a host of methods to determine the best fitting Gaussian LOSVD, such as the Fourier quotient method (Simkin 1974, Sargent et al 1977), modified by Winsall (1991) to incorporate also non-Gaussian LOSVDs, the cross correlation method (Tonry & Davis 1979), the Fourier fitting method (Franx, Illingworth & Heckman 1989) and the Fourier correlation quotient method (Bender 1990).

Motivated by the increasing quality of the data, new methods have been developed recently that are able to quantify symmetric and antisymmetric deviations of the LOSVD shape from a Gaussian (e.g. van der Marel & Franx 1993 and Gerhard 1993). A LOSVD is then parametrised by the average projected velocity $\langle v_p \rangle$, the projected dispersion σ_p and the lowest order coefficients of a Gauss-Hermite expansion of the LOSVD, h_3 and h_4 . These can subsequently be

used in a fitting routine to construct a dynamical model that best represents the kinematical data.

Another path leading to estimates of the shape of LOSVDs employs non-parametric fitting procedures such as the Wiener filtering method (Rix & White 1992), the maximum entropy method (Statler 1991), the unresolved Gaussian method (Kuijken & Merrifield 1993) and the Bayesian fitting method (Saha & Williams 1994). These give a totally unbiased estimate of the LOSVDs.

It is clear that all these modeling techniques require two fits. One fit is needed to extract the kinematics from the spectra, and a second fit then produces a dynamical model. In this paper we propose a method to construct a distribution function that operates directly on the available spectra, after they have undergone all the necessary steps of a standard data reduction. This problem is well defined, as is shown by Dejonghe & Merritt (1992). The essentials of the method are explained in the next section. In section 3, we test the method on a set of spherical anisotropic Plummer models.

2 THE MODELING PROCEDURE

A galaxy spectrum, obtained at a given position (x_p, y_p) on the sky, is the integrated light of all the stars along the line-of-sight. The spectrum of each contributing star is Doppler shifted according to its velocity relative to the observer. If we assume that the bulk of the light of the galaxy is produced by stars of approximately the same spectral class (in the case of an elliptical galaxy, most of the light originates from the G to M giants) we can write the following form for a

[★] Research Assistant of the Fund for Scientific Research - Flanders (Belgium)(F.W.O)

galaxy spectrum at (x_p, y_p)

$$g(x_p, y_p, \lambda) = \int \phi(v_p, x_p, y_p) s(\lambda(v_p)) dv_p \quad (1)$$

which expresses the spectrum as a sum of products of probabilities : the probability of finding a star with projected velocity v_p at a position (x_p, y_p) and the probability that such a (standard) star emits a photon with Doppler shifted wavelength λ , according to its spectrum in the rest frame $s(\lambda)$. We denote the rest wavelength by $\lambda(v_p)$. For velocities which are small compared to the velocity of light one has the Doppler shift formula

$$\frac{v_p}{c} = \frac{\lambda - \lambda(v_p)}{\lambda(v_p)} \approx \ln \frac{\lambda}{\lambda(v_p)}. \quad (2)$$

Obviously, (1) can be written in the form of a convolution using logarithmically rebinned spectra, which also eliminates the choice of a dimension for the wavelengths. Hence

$$g(x_p, y_p, \ln \lambda) = \int \phi(v_p, x_p, y_p) s(\ln \lambda - \frac{v_p}{c}) dv_p. \quad (3)$$

It is always possible to write the distribution function (hereafter DF) $F(\mathbf{I})$, where \mathbf{I} are the isolating integrals of the motion, as an infinite sum of basis functions $F^i(\mathbf{I})$ with coefficients c_i

$$F(\mathbf{I}) = c_i F^i(\mathbf{I}). \quad (4)$$

In the sequel, we will consistently use a summation convention. These basis functions are the DFs of simple dynamical models, called the components, that form a complete set. Denoting by v_x and v_y the velocity components in the plane of the sky, and by z the coordinate along the line-of-sight, we find formally

$$\phi(v_p, x_p, y_p) = \int_{-\infty}^{\infty} dz \iint F(\mathbf{I}) dv_x dv_y. \quad (5)$$

Obviously, the LOSVD is linear in the DF, and can also be written as a weighed sum of component LOSVDs $\phi^i(v_p, x_p, y_p)$ with the same coefficients c_i as the DF. Likewise, we obtain component spectra

$$g^i(x_p, y_p, \ln \lambda) = \int \phi^i(v_p, x_p, y_p) s(\ln \lambda - \frac{v_p}{c}) dv_p. \quad (6)$$

We label with the composite index n the k -th pixel of the l -th galaxy spectrum (we label each spectrum and its corresponding line-of-sight with a number l) and denote its value by g_n . A similar notation applies for the spectra of the i -th component, g_n^i . It is easy to see that ideally

$$g_n = c_i g_n^i \quad n = 1, \dots, N, \quad (7)$$

with N the total number of pixels considered.

Since we can only handle a truncated expansion of the DF, we will have to use a limited number m of components and try to find those coefficients c_i that give rise to a model that best represents the data. This we do by using a Quadratic Programming minimisation technique (Dejonghe 1989). The stellar template spectrum is normalised to one

$$\int_{-\infty}^{\infty} s(\ln \lambda) d \ln \lambda = 1, \quad (8)$$

where the function $s(\ln \lambda)$ is set to zero in the region outside the data. The aim is to model the observed spectra with (7).

Since the component LOSVDs $\phi^i(v_p, x_p, y_p)$ are normalised to their projected mass density $\rho_p^i(x_p, y_p)$, the calculated component spectra $g^i(x_p, y_p, \ln \lambda)$ will also be normalised to $\rho_p^i(x_p, y_p)$. In order to make (7) correct, in the sense that

$$\rho(x_p, y_p) = c_i \rho_p^i(x_p, y_p), \quad (9)$$

the observed galaxy spectra $g(x_p, y_p, \ln \lambda)$ must be normalised to the projected mass density $\rho_p(x_p, y_p)$. However, an observed galaxy spectrum cannot be written exactly as the convolution of a template spectrum and a LOSVD since such a convolution has two rapidly decaying wings in both regions where the template spectrum is unknown and by default set to zero. Observed galaxy spectra are also unknown and set to zero in the same regions as the template spectra. So by normalising the galaxy spectra to the projected mass density a small error is introduced, because the two small but unknown wings, required to make the convolution formally exact, are neglected.

Usually the continuum of a galaxy spectrum and the continuum of a weighed sum of component spectra will not be the same. That is why the continua of the galaxy spectra and the stellar template spectrum have to be subtracted before they are normalised. For simplicity, we still use the notation $g(x_p, y_p, \ln \lambda)$, now for a continuum subtracted galaxy spectrum, and $s(\ln \lambda)$ for the continuum subtracted stellar spectrum.

The quantity that has to be minimised is

$$\chi^2 = w^n (g_n - c_i g_n^i)^2, \quad (10)$$

with $w^n = 1/\sigma_n^2$ and σ_n the noise on g_n , which is well modeled by Poisson noise. This expression can be expanded into the form

$$\chi^2 = c_i D^{ij} c_j - 2p^i c_i + e \quad (11)$$

or, in matrix notation

$$\chi^2 = c^t \mathbf{D} c - 2\mathbf{p}^t c + e. \quad (12)$$

The matrix \mathbf{D} with elements

$$D^{ij} = w^n g_n^i g_n^j \quad (13)$$

is called the Hessian matrix and the vector \mathbf{p} has components

$$p^i = w^n g_n^i g_n. \quad (14)$$

The scalar constant e is given by

$$e = w^n g_n g_n. \quad (15)$$

This χ^2 is quadratic in the coefficients. It has to be minimised under the linear constraint that the DF has to be positive

$$c_i F^i(\mathbf{I}) \geq 0. \quad (16)$$

The positivity is tested on a grid in phase space. This is a typical problem of Quadratic Programming. Moreover, the χ^2 has the statistical meaning of a goodness of fit so its expectation value equals

$$\langle \chi^2 \rangle = N - m - 1. \quad (17)$$

Other observational data can be added to this χ^2 . However, it loses its meaning as a goodness of fit when other weights than the errors are used in (10). In appendix C we present the error analysis on the obtained coefficients.

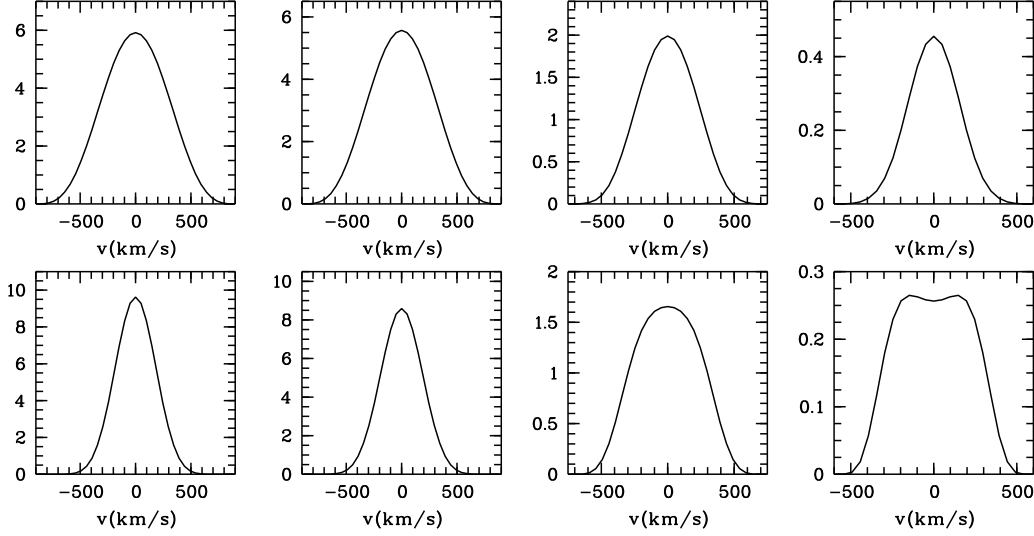


Figure 1. The LOSVDs of a radial Plummer model with $q = 1$ (top) and a tangential Plummer model with $q = -6$ (bottom), both with $M = 5 \times 10^{11} M_{\odot}$ and $r_c = c = 5$ kpc, for $r_p = 0, 1, 5$ and 10 kpc (from left to right).

3 PUTTING THE METHOD TO THE TEST

To test our modeling procedure we make use of synthetic galaxy spectra with simulated Poisson noise. These are created with spherical anisotropic Plummer models (Dejonghe 1987). The synthetic spectra are then used as input for our modeling procedure. As components we use generalised Fricke models.

3.1 The Plummer model

The Plummer potential can be written as

$$\psi(r) = \frac{GM}{r_c} \frac{1}{\sqrt{1 + (r/r_c)^2}} \quad (18)$$

with r_c the so-called core radius and M the total mass. We take $\sqrt{\psi(0)} = \sqrt{GM/r_c}$ as the unit of velocity so the central value of the potential becomes unity. The density of the anisotropic Plummer models can be written as

$$\rho(r) = \psi(r)^{5-q} (1 + (r/c)^2)^{-q/2} \quad (19)$$

with q and c real numbers. This function is an augmented mass density that is instrumental in the construction of the 2-integral DF $F(E, L)$ (Dejonghe 1986). Inserting the functional form for the Plummer potential in this expression, with $r_c = c$, one sees that all Plummer models have the same density distribution

$$\rho(r) = (1 + (r/c)^2)^{-5/2}. \quad (20)$$

We will approximate the anisotropic Plummer model with Fricke components with augmented mass density

$$\rho(r) = \psi(r)^{\alpha} (r/c)^{2\beta} \quad (21)$$

with α and β real numbers. The characteristics of both the Plummer models and the Fricke components can be calculated using a more general expression for the mass density

$$\rho(r) = \psi(r)^{\alpha} \left(\frac{r}{c}\right)^{2\beta} \left(1 + \left(\frac{r}{c}\right)^2\right)^{-(\beta+\gamma)} \quad (22)$$

with α , β and γ real numbers that satisfy

$$\alpha > 3 - 2\gamma \quad (23)$$

to keep the total mass finite. Choosing $\beta = 0$, $\alpha = 5 - q$ and $\gamma = q/2$ one recovers the density of the Plummer models. The choice $\gamma = -\beta$ yields the density of the Fricke components. The advantage of the above-mentioned family lies in the fact that most of the kinematics can be calculated analytically. This is for instance the case for the anisotropic velocity moments (see Appendix A)

$$\begin{aligned} \mu_{2n, 2m}(r) &= \mathcal{C}(m, n) \psi(r)^{\alpha+m+n} \frac{(r/c)^{2\beta}}{(1 + (r/c)^2)^{\beta+\gamma}} \times \\ &{}_2F_1(-m, \gamma + \beta; \beta + 1, \frac{(r/c)^2}{1 + (r/c)^2}) \end{aligned} \quad (24)$$

with

$$\mathcal{C}(m, n) = \frac{2^{m+n} \Gamma(n + 1/2) \Gamma(\alpha + 1) \Gamma(\beta + m + 1)}{\sqrt{\pi} \Gamma(\beta + 1) \Gamma(\alpha + m + n + 1)}. \quad (25)$$

This general expression yields the following expressions for the radial and tangential velocity dispersions,

$$\rho(r) \sigma_r^2(r) = \mu_{2,0}(r) = \frac{1}{1+\alpha} \psi(r)^{1+\alpha} \frac{(r/c)^{2\beta}}{(1 + (r/c)^2)^{\beta+\gamma}} \quad (26)$$

$$\begin{aligned} \rho(r) \sigma_{\phi}^2(r) &= \rho(r) \sigma_{\theta}^2(r) = \frac{1}{2} \mu_{0,2}(r) = \frac{1+\beta}{1+\alpha} \psi(r)^{1+\alpha} \times \\ &\frac{(r/c)^{2\beta}}{(1 + (r/c)^2)^{\beta+\gamma}} \left(1 - \frac{\gamma + \beta}{1 + \beta} \frac{(r/c)^2}{(1 + (r/c)^2)}\right). \end{aligned} \quad (27)$$

Binney's anisotropy parameter then reads

$$\beta(r) = 1 - \frac{\sigma_{\phi}^2}{\sigma_r^2} = \frac{-\beta + \gamma(r/c)^2}{1 + (r/c)^2}. \quad (28)$$

For a detailed derivation of the anisotropic velocity moments, we refer to appendix A.

One easily sees that the Fricke components have a constant anisotropy

$$\beta(r) = -\beta. \quad (29)$$

The tangentially anisotropic components have zero central density whereas the radially anisotropic ones have a central

density cusp. The isotropic components have a nonzero and finite central density. For the Plummer models

$$\beta(r) = \frac{q}{2} \frac{(r/c)^2}{1 + (r/c)^2}. \quad (30)$$

We see that $\beta(r)$ and q have the same sign and since $-\infty < \beta(r) < 1$ the allowed range for q is $-\infty < q < 2$. The true nature of the orbital structure of a model becomes clearly visible in the kinematics at radii $r \geq c$.

A LOSVD of a tangential Plummer model along a line-of-sight close to the center is narrow and peaked. Moving the line-of-sight outward, the LOSVDs become progressively broader and ultimately obtain a bimodal shape. The LOSVDs of a radial model, on the contrary, will be broader towards the center and narrower at large projected radii. As an illustration, Fig. 1 shows the LOSVDs of a radial Plummer model with $q = 1$ (top) and a tangential Plummer model with $q = -6$ (bottom) for $r_p = 0, 1, 5$ and 10kpc.

3.2 The synthetic spectra

We want to construct spectra with (3) so it is important that we can calculate the necessary LOSVDs efficiently. It turns out that for a subset of the models one can perform the integrations of the DF over the velocity components in the plane of the sky analytically. This yields $lp(r, r_p, v_p)$, the probability of finding a star with projected velocity v_p at a distance r from the center of the cluster and on a line-of-sight at a distance r_p in the plane of the sky from the center. The following expression is valid only when β is a positive integer and $\beta + \gamma$ a negative integer (see Appendix B) :

$$\begin{aligned} lp(r, r_p, v_p) &= \frac{1}{\sqrt{2\pi}} \frac{\Gamma(\alpha + 1)}{\Gamma(\alpha + 1/2)} \frac{(r/c)^{2\beta}}{(1 + (r/c)^2)^{\beta + \gamma}} \times \\ &\psi(r)^{\alpha - 1/2} \sum_{j=0}^{-(\beta + \gamma)} (\beta + \gamma)_j \frac{\xi^j}{j!} (\sin \eta)^{2j} \times \\ &\sum_{i=0}^{\beta} \left(\frac{1}{2}\right)_{i+j} \frac{(-\beta)_i}{(i+j)!} \left(1 - \frac{v_p^2}{2\psi(r)}\right)^{-(i+j) + \alpha - 1/2} \times \\ &\frac{(\sin \eta)^{2i}}{i!} {}_2F_1(-i+j, \alpha; \frac{1}{2}; \frac{v_p^2}{2\psi(r)}). \end{aligned} \quad (31)$$

Here

$$\xi = \frac{(r/c)^2}{1 + (r/c)^2} \quad (32)$$

and $\eta(r, r_p)$ is the angle between the spherical radial direction and the line-of-sight at a certain point of the line-of-sight. The integration along the line-of-sight has to be performed numerically. The LOSVDs of the models we use are particularly simple. In the case of Fricke components the above expression is reduced to a sum over i , for Plummer models a sum over j remains. LOSVDs of models that do not have positive integer β or negative integer $\beta + \gamma$ have to be calculated numerically using (5).

We calculate spectra out to about two effective radii. For a de Vaucouleurs law, a distance of two effective radii encloses approximately 69% of the total luminosity. For a Plummer galaxy this corresponds to $r_p = 1.49c$.

Besides a LOSVD, one also needs a stellar template spectrum to construct a galaxy spectrum. We use the spec-

trum of the K giant HR2425 in a wavelength range from 3900Å to 5400Å. This spectrum is rebinned logarithmically so that one pixel corresponds to a velocity interval of 52 km/s. The Gaussian width (σ_{instr}) of a line that is intrinsically a delta function is about 150 km/s. The synthetic spectra are calculated with (3) and noise is added according to a specified S/N ratio.

3.3 Testing the method

To test if our modeling procedure can successfully perform the inversion of the integral equation (3) we offer the program noisy synthetic spectra of a Plummer galaxy. We assume that the Plummer galaxy contains only stars of the same spectral class. In that case it is not necessary to subtract the continuum of the spectra. We also use the stellar spectrum with which the synthetic spectra are created as a template spectrum. These assumptions are needed to avoid problems with bad continuum subtraction, template mismatch etc. that have only to do with the data reduction and are common to all methods. Due to the normalisation of the template spectrum and the LOSVDs, the synthetic spectra will have automatically the proper normalisation (see the discussion about the normalisation of spectra in the paragraph below equation (8)).

3.3.1 A tangential $q = -2$ Plummer galaxy

We first consider a mildly tangential $q = -2$ Plummer model. The model has a core radius $r_c = c = 6.75\text{kpc}$ and a total mass of $6.5 \times 10^{11} M_{\odot}$. This galaxy is placed at a distance of 206265 kpc so that one arc-second (") on the sky corresponds to a distance of 1 kpc. Two effective radii correspond to approximately 10" so we generate spectra for $r_p = 0'', 0.5'', 1'', \dots, 10''$. We only use a wavelength interval of about 170Å containing the *MgI* lines around 5180Å and a strong *FeII* line at 5270Å. During the fit, the correct mass and Plummer potential are adopted.

The augmented mass density of this Plummer model can be written as a binomial expansion, which shows that it can in principle be fitted exactly in terms of Fricke components with $\alpha = 7$. We first offer the routine noiseless data. A library is set up that contains the Fricke components with $\alpha = 4, 5, 6, 7, 8, 10$ and 12 and with positive integer β . These components are chosen because they span a wide range in dynamical behavior. The models with high α -values are more centrally concentrated. The higher the value of β the more tangentially anisotropic the component becomes. When dealing with real data, one has to make a reasonable choice of components. In the following we will only use Fricke components with positive integer β . This is just to save calculation-time : the LOSVDs of these components can be calculated analytically.

The 'redundant' components do not contribute significantly to the result (they are not chosen or else given a very small coefficient) and the correct components have the right coefficients. Thus, the input model can be successfully recovered, which is of course a prerequisite.

We now consider data with a signal to noise ratio of $S/N \approx 80$ in the center, dropping to $S/N \approx 25$ at two effective radii. Here and in the following, all signal to noise

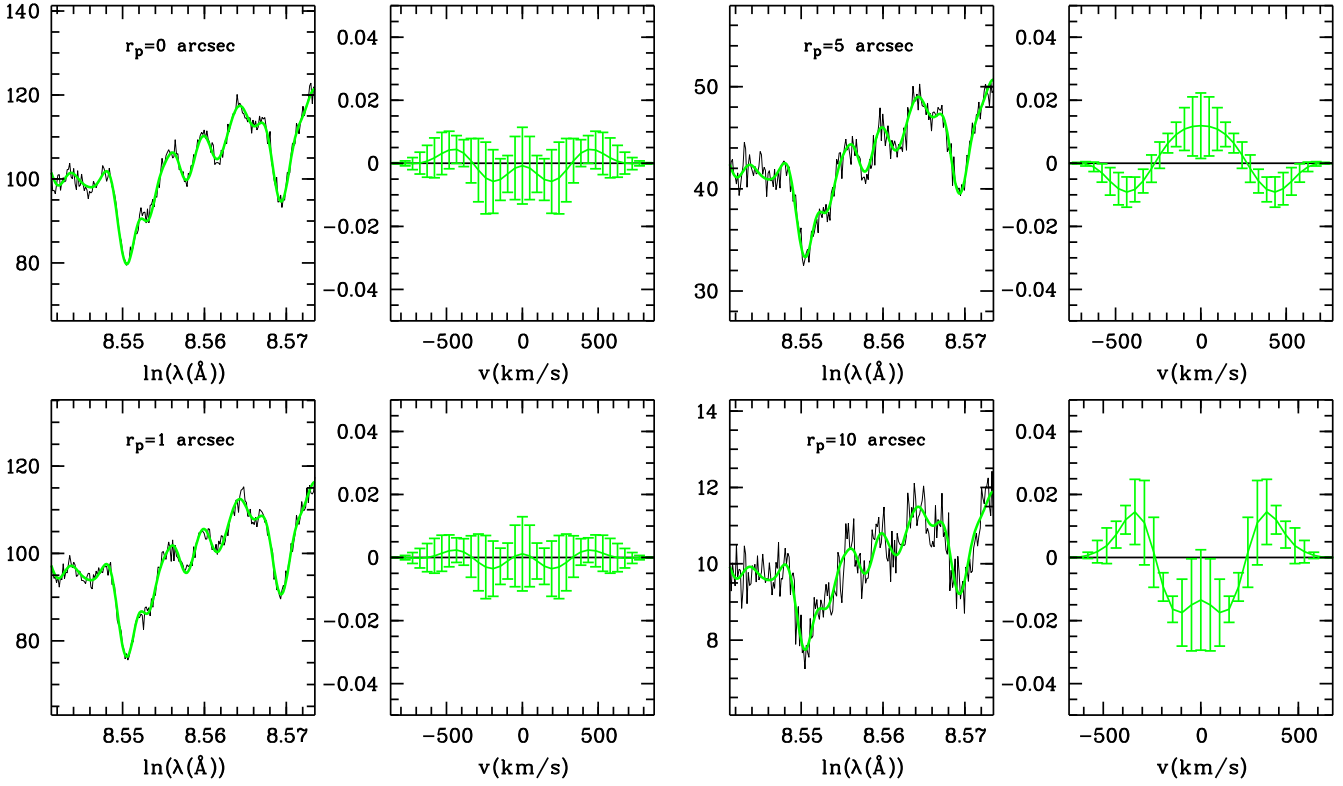


Figure 2. The synthetic spectra of a tangential $q = -2$ Plummer galaxy (black) with central $S/N \approx 80$ for four different lines-of-sight. The scaling of the ordinate is arbitrary. Over-plotted in grey is the best fitting spectrum (the Fricke components with $\alpha = 4, 5, 6, 8, 9, 10$ and 12 are used). To the right of each spectrum, we plotted $(\phi(\text{theo}) - \phi(\text{fit})) / \phi(\text{theo})_{\text{max}}$ with $\phi(\text{theo})$ the Plummer LOSVD, $\phi(\text{fit})$ the fitted LOSVD and $\phi(\text{theo})_{\text{max}}$ the top value of the Plummer LOSVD. One can see that the deviations between the Plummer LOSVD and the fitted LOSVD are nowhere larger than 1 to 2 % of the top value.

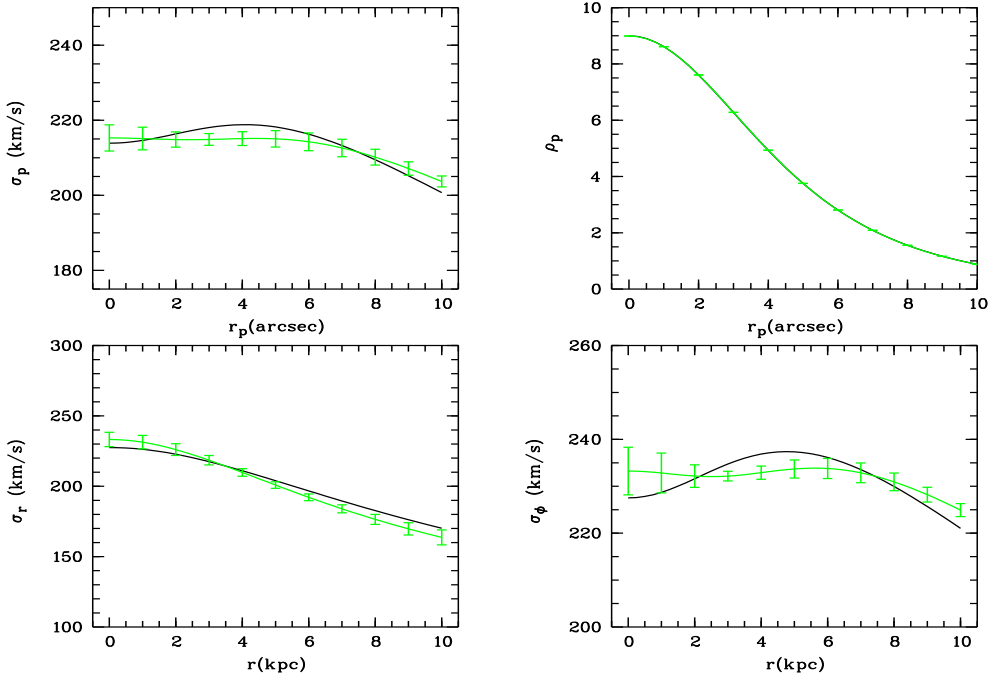


Figure 3. The kinematics of a tangential $q = -2$ Plummer galaxy (black). Clockwise are plotted the projected velocity dispersion $\sigma_p(r_p)$, the projected mass density $\rho_p(r_p)$ (in dimensionless units), the tangential velocity dispersion $\sigma_\phi(r) = \sigma_\theta(r)$ and the radial velocity dispersion $\sigma_r(r)$. Shown in grey are the kinematics derived from the best fitting model (using data with central $S/N \approx 80$ and Fricke components with $\alpha = 4, 5, 6, 8, 9, 10$ and 12). The deviations are of the order of 5 km/s. The errorbars give a fair idea of the actual errors on these derived quantities. There is one active constraint.

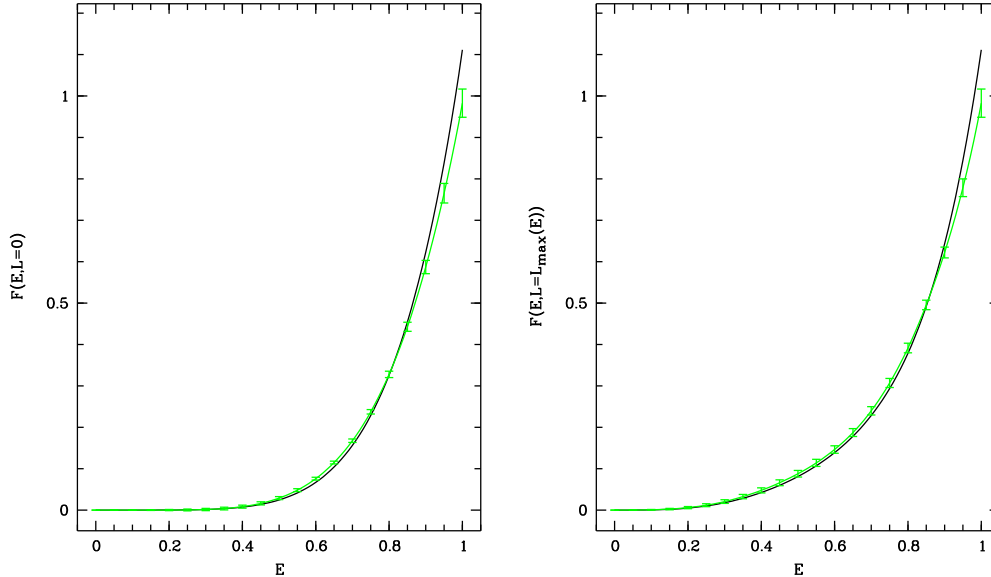


Figure 4. The DF of a $q = -2$ Plummer galaxy (black) and the fitted DF (grey), with errorbars, shown for $L = 0$ (left) and $L = L_{max}(E)$ (right). The fitted DF results from a fit to data with maximum $S/N \approx 80$. Fricke components with $\alpha = 4, 5, 6, 8, 9, 10$ and 12 are used. There is only one active constraint.

values are expressed per pixel. The Fricke components with $\alpha = 4, 5, 6, 7, 8, 10$ and 12 again serve as components. It appears that the spectra constrain the LOSVDs to a high degree. The routine still uses the correct components and assigns to them approximately the correct coefficients but now also uses a few other components to reach a minimum χ^2 . A more objective test is to fit the data without incorporating the components that can represent the Plummer model exactly in the library. The spectra are now fitted with a library containing the Fricke components with $\alpha = 4, 5, 6, 8, 9, 10$ and 12 . This also gives an accurate approximation of the LOSVDs (see Fig. 2). Although they are not included in the fit, the observables $\sigma_p(r_p)$ and $\rho_p(r_p)$ are very well recovered (see Fig. 3).

One can also use the errors on the coefficients to estimate the uncertainty on the DF itself. Fig. 4 shows the DF of the $q = -2$ Plummer model and the DF that results of the previous fit. The left plot shows a cut through the DF at $L = 0$, the radial orbits. The right one displays a cut along $L = L_{max}(E)$, the maximum angular momentum an orbit with a certain energy can have, which is the locus of the circular orbits. It can be seen that the fitted DF closely follows the Plummer DF. Only in the center, where the DF is rather peaked, is there a noticeable difference.

When spectra are used with $S/N \approx 55$ in the central regions, dropping to $S/N \approx 15$ at two effective radii, the method still yields a good approximation to the Plummer model (see Fig 5 and 6). Fig. 7 compares the Plummer DF with the fitted DF. There are no active constraints. The deviations between the kinematics of the fitted model and of the Plummer galaxy are larger but the errorbars, indicating the uncertainty on the coefficients, are accordingly larger.

The analysis of about 20 spectra, each spanning a spectral region of $\approx 200\text{\AA}$, with the limited number of components used here, takes only a few hours on a Pentium II (this

is the time needed to calculate all the component spectra and to do the fit).

3.3.2 Testing the errorbars

To test if the errorbars give a reliable idea of the 1σ uncertainty on the coefficients, we construct 40 sets of 21 synthetic spectra with $r_p = 0'', 0.5'', 1'', \dots, 10''$ and a $S/N \approx 80$ at $r_p = 0''$. The spectra are generated with the $q = -2$ Plummer model of the previous paragraph.

To each of these sets a model is fitted, using the Fricke components $\alpha = 4, 6, 7, 8$ and 10 with positive integer β and assuming the correct Plummer potential and mass. We then calculate for $r_p = 0'', 1'', 5''$ and $10''$ and for selected v_p the mean and the dispersion (this we call the experimental dispersion) of the LOSVDs of those 40 models. The average LOSVDs tend towards the true LOSVDs and the 'experimental' and the theoretical 1σ -errorbars essentially coincide, as can be seen in Fig. 8. Hence, the errorbars are a reliable measure for the possible spread between the input model and a typical fit, as caused by the adopted Poisson noise. One also concludes that if the used component library is sufficiently complete the systematic errors are negligible, compared to the random errors caused by the Poisson noise.

3.3.3 A tangential $q = -6$ Plummer galaxy

This is a fairly tangential model. With the choice $r_c = c = 5$ kpc, the bimodal structure will reveal itself at $r_p \geq 5''$. The mass is $5 \times 10^{11} M_\odot$. Two effective radii now correspond to $7.5''$. Spectra are generated for $r_p = 0'', 0.5'', 1'', \dots, 7.5''$, once with a central $S/N \approx 80$ and once with a maximum $S/N \approx 55$. This Plummer model can be written exactly as a weighed sum of the four Fricke components with $\alpha = 11$.

The Fricke models with $\alpha = 7, 9, 10, 11, 12, 13$ and 14 serve as components. The routine does not recognise the

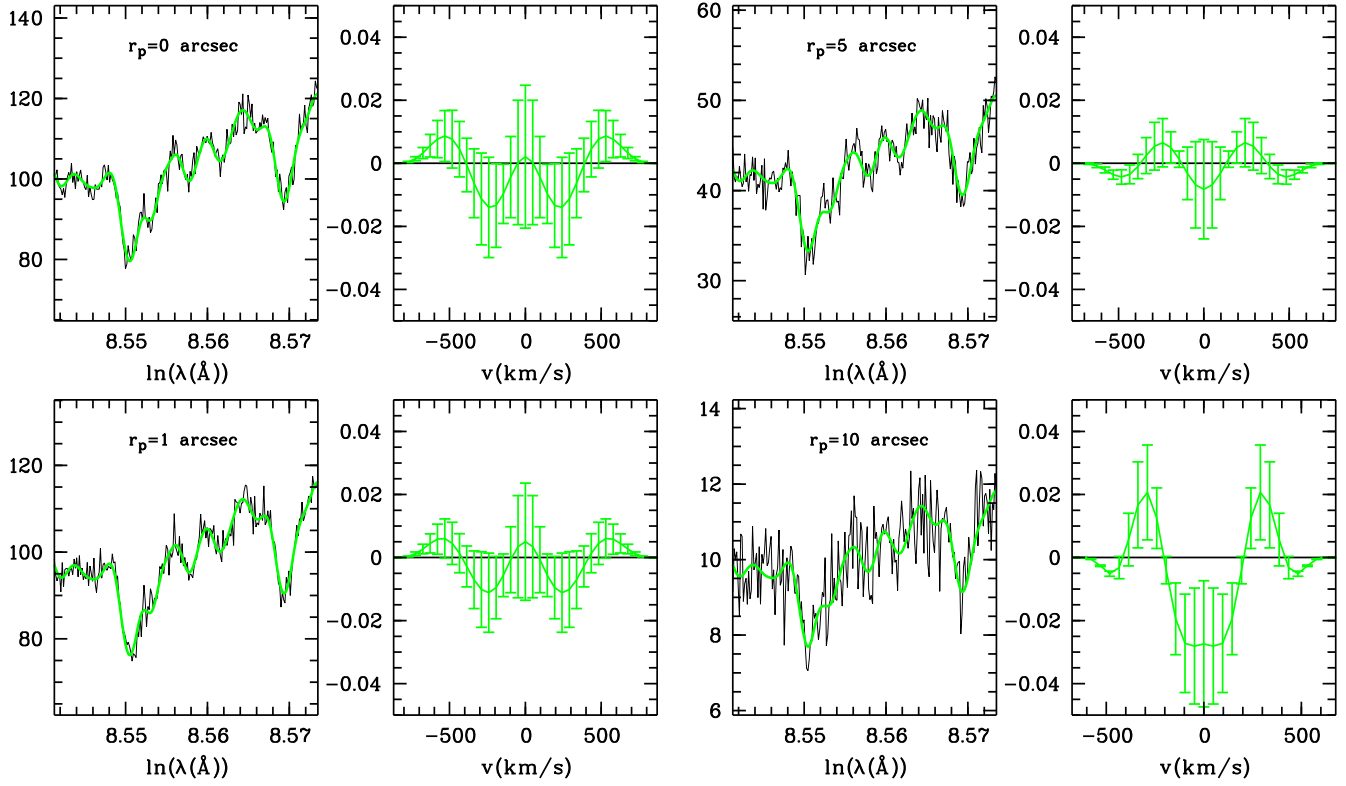


Figure 5. The same as Fig. 2 but for a fit to data with central $S/N \approx 55$, using the same Fricke components. There are no active constraints.

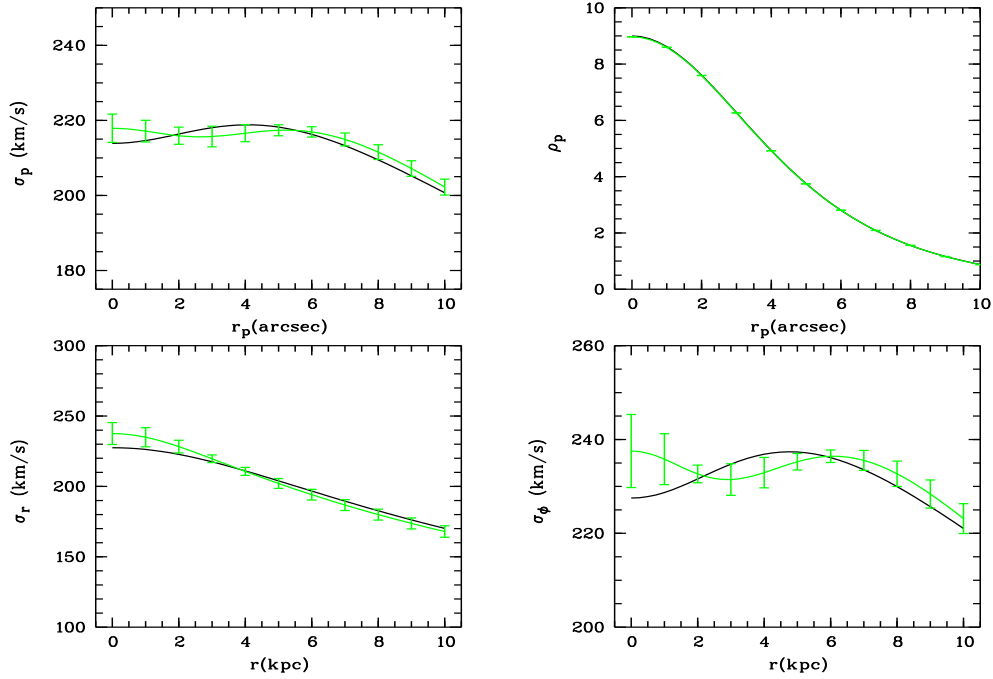


Figure 6. The same as Fig. 3 but for a fit to data with maximum $S/N \approx 55$, using the same Fricke components. There are no active constraints.

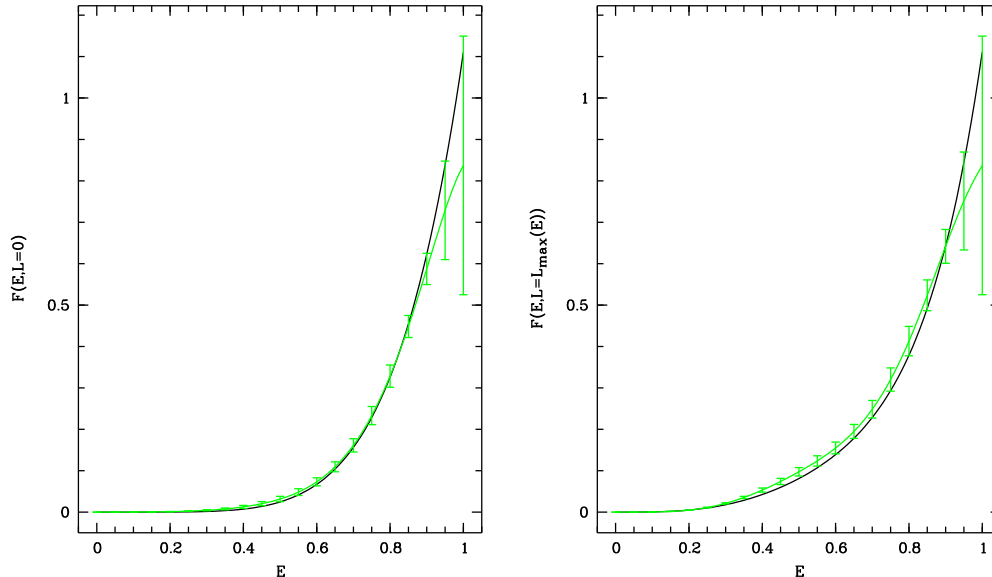


Figure 7. The same as Fig. 4 but for a fit to data with maximum $S/N \approx 55$.

Fricke components with $\alpha = 11$ as the correct ones. They appear in the weighed sum with a coefficient that is totally different from the one that would be expected from the binomial expansion of the augmented mass density. It is possible to obtain a very good fit to the data (see Fig. 9 and Fig. 10 for data with a central $S/N \approx 80$). The LOSVDs (including the bimodal shape at large radii) and the kinematics are very well reproduced. Fig. 11 compares the Plummer DF and the fitted DF. There are no active constraints.

3.3.4 A radial $q = 1$ Plummer galaxy

A radial model has much broader LOSVDs in the center than a tangential model with the same mass. In the outer regions the inverse is true. As a consequence, the outer spectra of a radial model still contain some details that are totally smoothed out in the tangential models. Therefore the inversion of the convolution integral (3) is better behaved and the LOSVDs of a radial model are better constrained by the data at large r_p than those of a tangential one. This Plummer model has $r_c = c = 5$ kpc and a total mass of $5 \times 10^{11} M_\odot$. Spectra are generated for $r_p = 0'', 0.5'', 1'', \dots, 7.5''$, once with a central $S/N \approx 80$ and once with $S/N \approx 55$. As components we use Fricke components with $\alpha = 4, 5, 6, 7$ and 8 .

The LOSVDs of this model cannot be written exactly as a weighed sum of Fricke components. Nonetheless, the LOSVDs are recovered very well in both cases (see Fig. 12 and 13). This is remarkable, because all components are either isotropic or tangential. The only way to construct a radial model with these components is to give tangential components a negative coefficient to suppress the number of stars on quasi-circular orbits.

Fig. 14 compares the Plummer DF and the fitted DF and shows the estimated 1σ deviation between both DFs.

4 CONCLUSION

As a conclusion we can state that the method can successfully perform the inversion of equation (3), given spectra of high enough quality (central signal to noise ratio equal to about 50 or higher) and the correct potential. The errorbars that can be derived from the Hessian matrix have a statistical meaning and give a good idea of the uncertainty on the fitted model.

This feature is probably the most important advantage of the present method. Up to now questions about the reliability of the inferred dynamics or the adopted potential have remained largely unanswered. With the present method, there is a link with the S/N of the data, the choice of the template spectra and the continuum subtraction, which may all have critical repercussions on the inferred models. Moreover, some simple form of population synthesis may be attempted for the best constrained models and geometries.

In recent years, a lot of researchers have addressed the important subject of constraining the potential of invisible matter (i.e. dark halo matter, central black holes), using kinematical data (e.g. Merritt & Oh (1996) (who use velocity dispersion data), Rix et al. (1997) (who use h_3 and h_4 in addition to projected streaming velocities and dispersions) and Gerhard et al. (1997) (who use h_4 and velocity dispersions)). It is not surprising that the inclusion of LOSVD shape parameters such as h_3 and h_4 in a modeling procedure, in addition to projected streaming velocities and dispersions, gives a significant improvement in determining the potential. Since in the present method one uses in fact all the information on the shape of the LOSVDs that can be learned from the spectra, it should be a valuable tool to constrain the shape and extent of the potential.

APPENDIX A: THE ANISOTROPIC VELOCITY MOMENTS

The anisotropic velocity moments

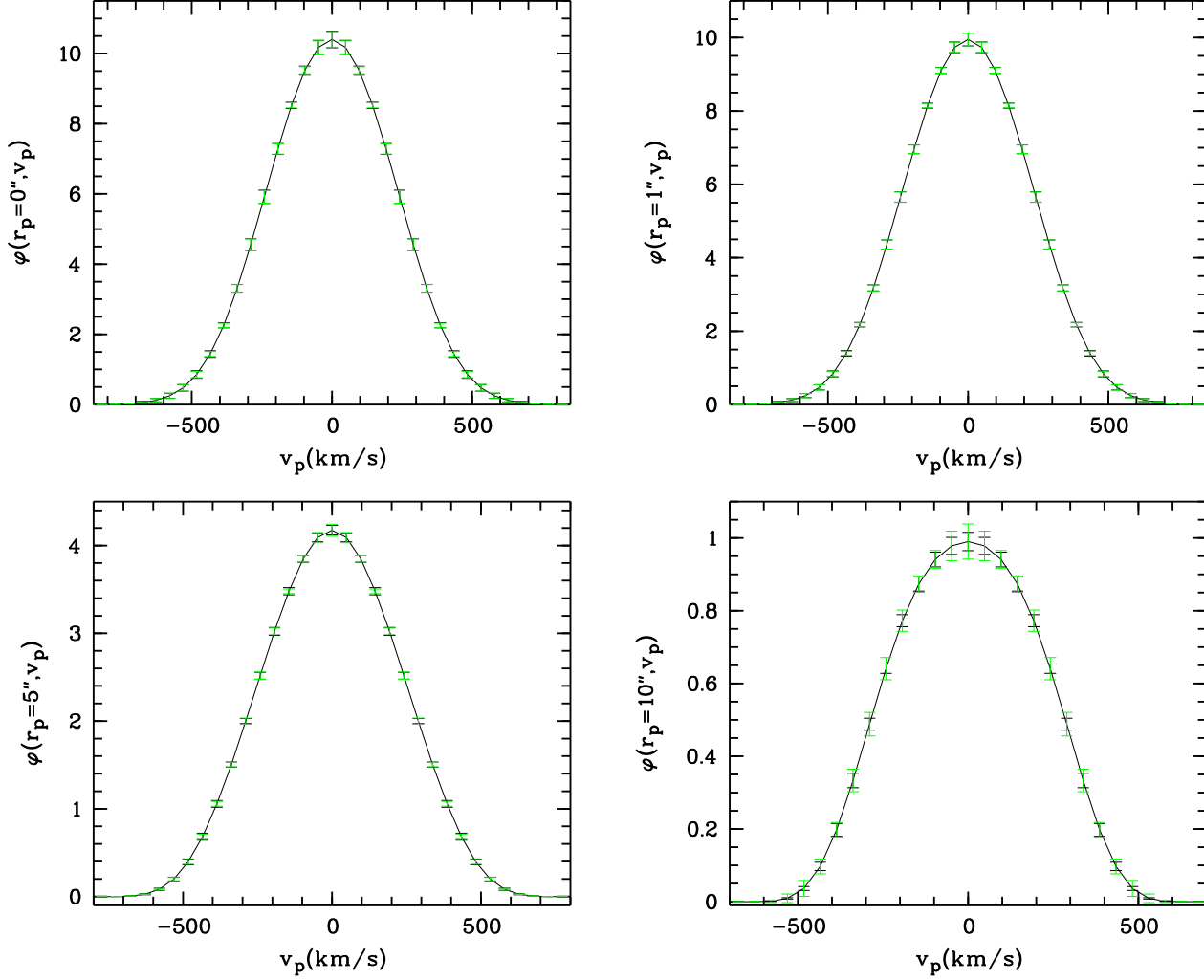


Figure 8. The average LOSVDs for $r_p = 0''$, $1''$, $5''$ and $10''$. Experimental (black) and theoretical (grey) 1σ errorbars are superposed. Where the errorbars coincide, the grey ones hide the black ones. Three positivity constraints are active.

$$\mu_{2n,2m}(r) = 2\pi \iint F(E, L) v_r^{2n} v_T^{2m} dv_r dv_T, \quad (\text{A1})$$

with $L = rv_T$ and $E = \psi(r) - \frac{1}{2}(v_r^2 + v_T^2)$ where $v_T = \sqrt{v_\phi^2 + v_\theta^2}$, are connected with the true velocity moments

$$\mu_{2n,2i,2j}(r) = \iiint F(E, L) v_r^{2n} v_\phi^{2i} v_\theta^{2j} dv_r dv_\phi dv_\theta \quad (\text{A2})$$

through the relation

$$\mu_{2n,2i,2j}(r) = \frac{1}{\pi} B\left(i + \frac{1}{2}, j + \frac{1}{2}\right) \mu_{2n,2(i+j)}(r). \quad (\text{A3})$$

It can be shown (Dejonghe 1986) that

$$\mu_{2n,2m}(r) = \frac{2^{n+m}}{\sqrt{\pi}} \frac{\Gamma(n + \frac{1}{2})}{\Gamma(n+m)} \times \int_0^{\psi(r)} (\psi(r) - \psi')^{n+m-1} D_{r^2}^m (r^{2m} \tilde{\rho}(\psi', r)) d\psi' \quad (\text{A4})$$

with $\tilde{\rho}(\psi, r)$ the augmented mass density, i.e. the density expressed as a function of r and ψ , the potential. Inserting

(22) for the mass density one finds

$$\mu_{2n,2m}(r) = \frac{2^{n+m}}{\sqrt{\pi}} \psi(r)^{\alpha+n+m} \frac{\Gamma(n + \frac{1}{2}) \Gamma(\alpha + 1)}{\Gamma(\alpha + n + m + 1)} \times D_x^m \left(\frac{x^{m+\beta}}{(1+x)^{\beta+\gamma}} \right) \quad (\text{A5})$$

with $x = (r/c)^2$. Since

$$\begin{aligned} D_x^m \left(\frac{x^{m+\beta}}{(1+x)^{\beta+\gamma}} \right) &= (-1)^m \frac{x^\beta}{(1+x)^{\beta+\gamma}} \times \\ &\sum_{j=0}^m \binom{m}{j} (-m-\beta)_{m-j} (\beta+\gamma)_j \left(\frac{x}{1+x} \right)^j \\ &= \frac{\Gamma(m+\beta+1)}{\Gamma(\beta+1)} \frac{(r/c)^{2\beta}}{(1+(r/c)^2)^{\beta+\gamma}} \times \\ &{}_2F_1(-m, \gamma+\beta; 1+\beta; \frac{(r/c)^2}{1+(r/c)^2}) \end{aligned} \quad (\text{A6})$$

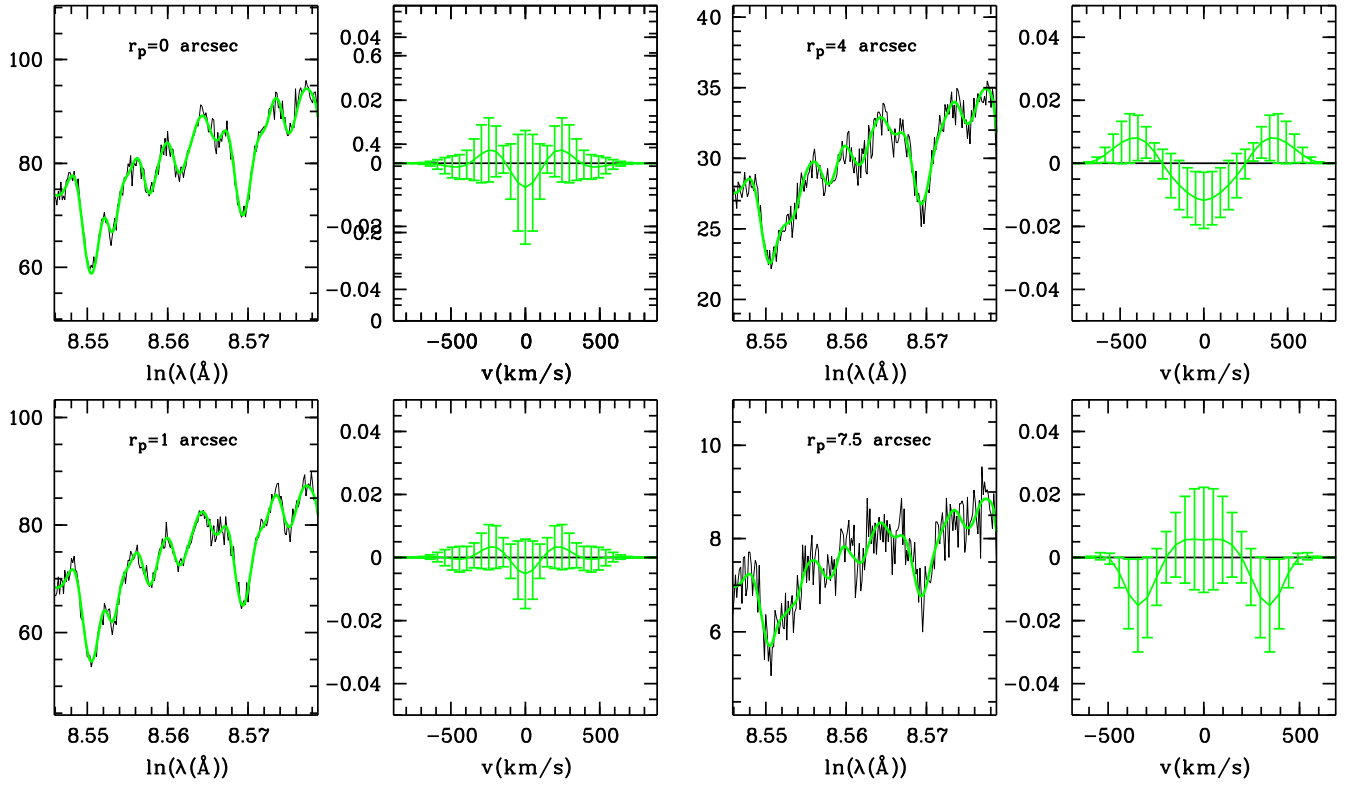


Figure 9. The same as in Fig. 2, but now for a tangential $q = -6$ Plummer galaxy. The Fricke components with $\alpha = 7, 9, 10, 11, 12, 13$ and 14 are used in a fit to data with $S/N \approx 80$ for $r_p = 0''$.

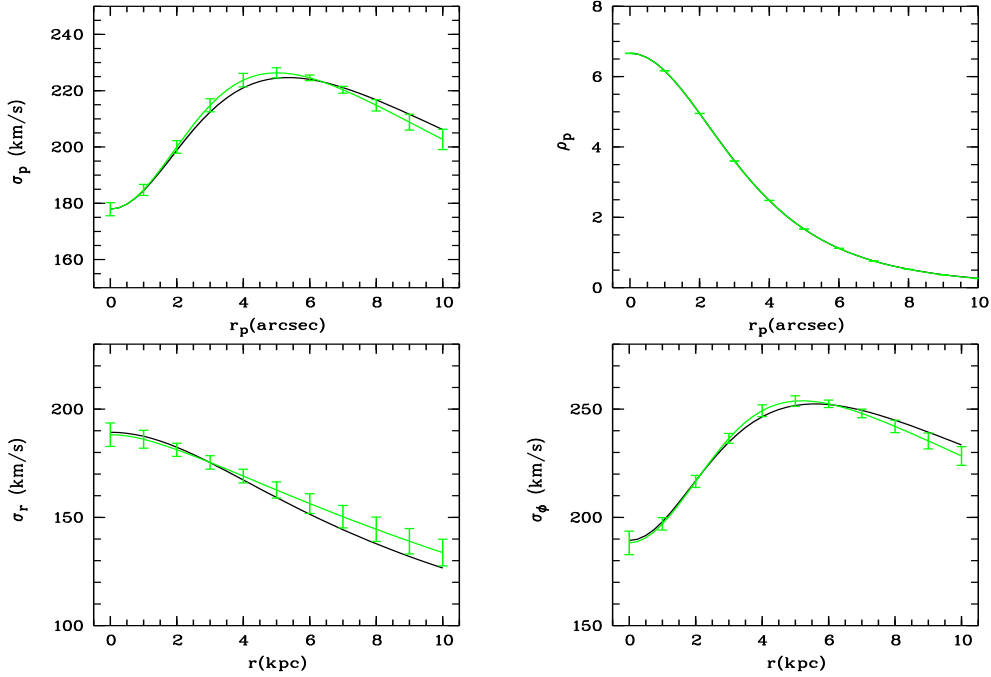


Figure 10. The same as in Fig. 3, but now for data from a tangential $q = -6$ Plummer galaxy with maximum $S/N \approx 80$.

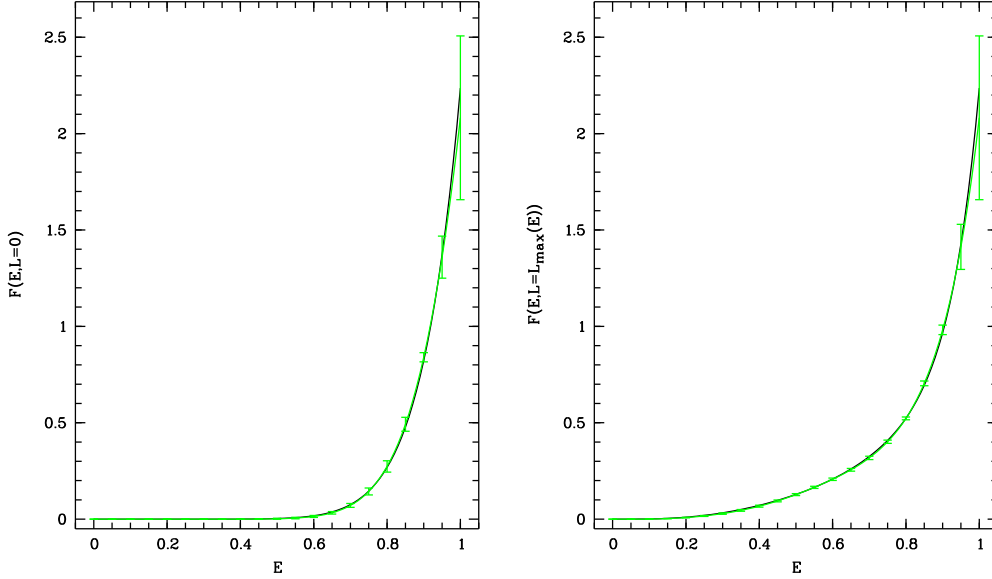


Figure 11. The same as Fig. 4 but for a tangential $q = -6$ Plummer galaxy.

the expression for the velocity moments can be rearranged as follows

$$\begin{aligned} \mu_{2n, 2m}(r) &= \frac{2^{n+m} \Gamma(n + \frac{1}{2}) \Gamma(\alpha + 1) \Gamma(\beta + m + 1)}{\sqrt{\pi} \Gamma(\beta + 1) \Gamma(\alpha + n + m + 1)} \times \\ &\psi(r)^{\alpha+n+m} \frac{(r/c)^{2\beta}}{(1 + (r/c)^2)^{\beta+\gamma}} \times \\ &{}_2F_1(-m, \gamma + \beta; 1 + \beta; \frac{(r/c)^2}{1 + (r/c)^2}). \end{aligned} \quad (\text{A7})$$

APPENDIX B: THE LOSVDS

To calculate the LOSVDs we make use of the fact that the Laplace transformation of a function $f(x)$ can be written as a power series containing the moments of that function $\mu_n = \int_0^\infty x^n f(x) dx$:

$$\mathcal{L}_{x \rightarrow s}\{f\} = \sum_{n=0}^{\infty} \frac{\mu_n}{n!} (-s)^n. \quad (\text{B1})$$

The aim is to calculate $lp(r, r_p, v_p)$, the probability of finding a star with projected velocity v_p at a distance r from the center of the cluster and on a line-of-sight with distance r_p to the center of the galaxy, which has only non-zero even moments

$$\begin{aligned} \mu_{2n}(r, r_p) &= \rho(r) \langle v_p^{2n}(r, r_p) \rangle \\ &= \sum_{i=0}^n \binom{2n}{2i} (\cos \eta)^{2(n-i)} (\sin \eta)^{2i} \times \\ &\mu_{2(n-i), 2i, 0}(r) \end{aligned} \quad (\text{B2})$$

with $\eta(r, r_p)$ the angle between the spherical radial direction and the line-of-sight at a point of the line-of-sight. Using the above derived expressions for the velocity moments this becomes

$$\mu_{2n}(r, r_p) = \frac{2^n \Gamma(n + \frac{1}{2}) \Gamma(\alpha + 1)}{\sqrt{\pi} \Gamma(n + \alpha + 1)} \frac{(r/c)^{2\beta}}{(1 + (r/c)^2)^{\beta+\gamma}} \times$$

$$\begin{aligned} &\psi(r)^{n+\alpha} \sum_{i=0}^n \binom{n}{i} (-1)^i (\sin \eta)^{2i} \times \\ &\sum_{j=0}^n \frac{(-\beta)_{i-j} (\beta + \gamma)_j}{j!(i-j)!} \xi^j \end{aligned} \quad (\text{B3})$$

with $\xi = (r/c)^2 / (1 + (r/c)^2)$. The Laplace transformation of $lp(r, r_p, v_p^2)$, for which we use the notation \mathcal{L} , can be written as

$$\begin{aligned} \mathcal{L} &= \mathcal{Q} \sum_{n=0}^{\infty} \frac{\Gamma(n + \frac{1}{2})}{\Gamma(n + \alpha + 1)} \frac{(-2\psi s)^n}{n!} \sum_{i=0}^n \binom{n}{i} \times \\ &(-1)^i (\sin \eta)^{2i} \sum_{j=0}^i \frac{(-\beta)_{i-j} (\beta + \gamma)_j}{j!(i-j)!} \xi^j \\ &= \mathcal{Q} \sum_{j=0}^{\infty} (\beta + \gamma)_j \frac{\xi^j}{j!} (\sin \eta)^{2j} \sum_{i=0}^{\infty} (-1)^{i+j} \frac{(-\beta)_i}{i!} \times \\ &\frac{(\sin \eta)^{2i}}{(i+j)!} \frac{\Gamma(i+j + \frac{1}{2})}{\Gamma(i+j + \alpha + 1)} (-2\psi s)^{i+j} \times \\ &{}_1F_1(i+j + \frac{1}{2}; i+j + \alpha + 1; -2\psi s). \end{aligned} \quad (\text{B4})$$

with

$$\mathcal{Q} = \frac{\Gamma(\alpha + 1)}{\sqrt{\pi}} \psi(r)^\alpha \frac{(r/c)^{2\beta}}{(1 + (r/c)^2)^{\beta+\gamma}}. \quad (\text{B5})$$

Making use of the fact that

$$\begin{aligned} \mathcal{L}_{y \rightarrow t}^{-1}\{ {}_1F_1(a; b; -y) \} \\ &= \frac{\Gamma(b)}{\Gamma(a)\Gamma(b-a)} (1-t)^{b-a-1} t^{a-1} \quad 0 < t < 1 \end{aligned} \quad (\text{B6})$$

$$= 0 \quad t > 1 \quad (\text{B7})$$

and

$$\mathcal{L}_{y \rightarrow t}^{-1}\{ y^k \mathcal{L}_{t \rightarrow y}\{f\} \} = f^{(k)}(t) +$$

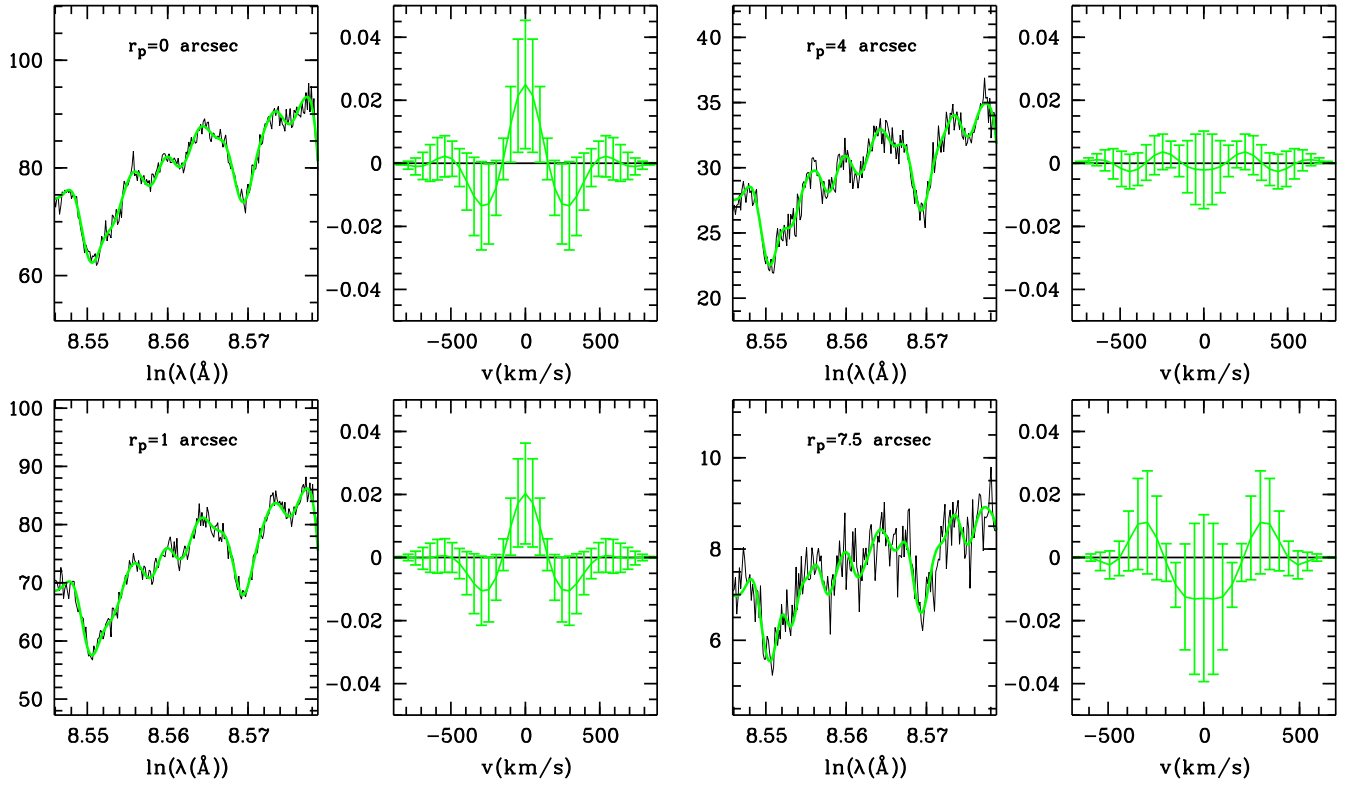


Figure 12. The same as in Fig. 2, but now for data from a radial $q = 1$ Plummer galaxy with maximum $S/N \approx 80$. We used Fricke components with $\alpha = 4, 5, 6, 7$ and 8 . There are no active constraints.

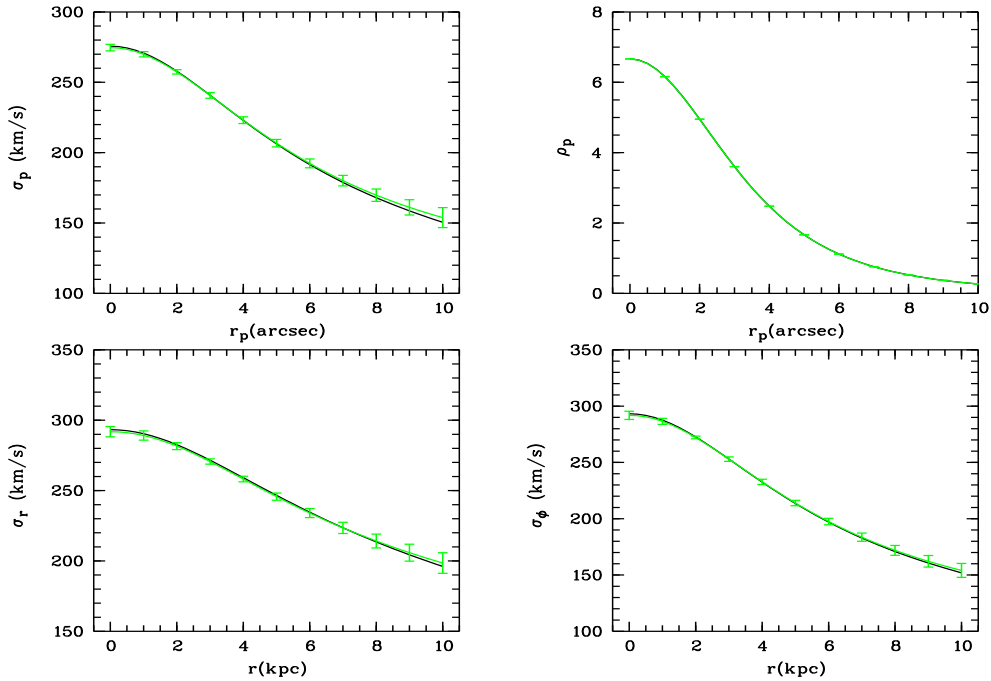


Figure 13. The same as in Fig. 3, but now for a radial $q = 1$ Plummer galaxy. There are no active constraints.

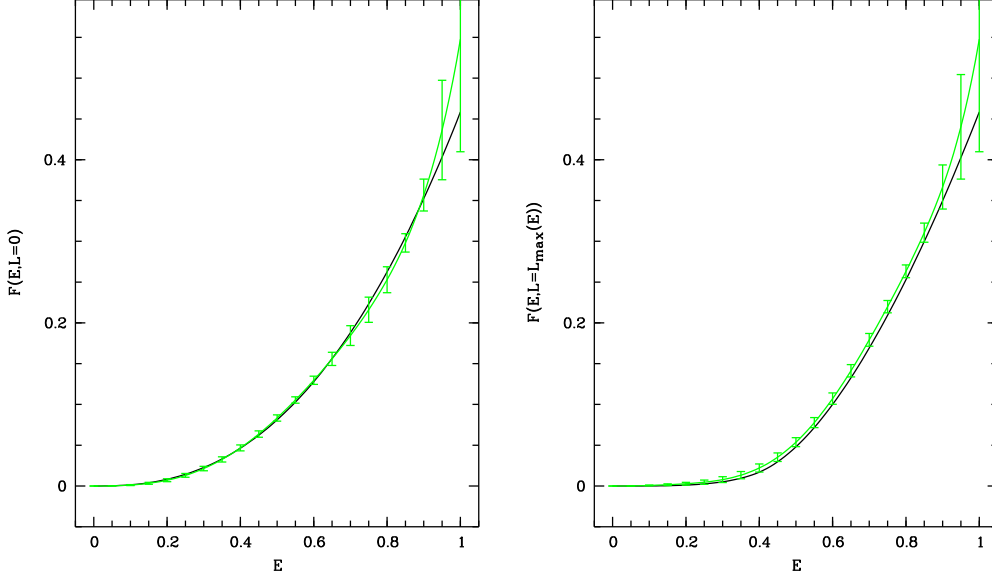


Figure 14. The same as Fig. 4 but for a radial $q = 1$ Plummer galaxy. There are no active constraints. The data used in the fit have maximum $S/N \approx 80$.

$$\sum_{n=1}^k f^{(k-n)}(0) \mathcal{L}_{y \rightarrow t}^{-1} \{y^{n-1}\}, \quad (\text{B8})$$

where $f^{(k)}$ stands for the k -th order derivative, one can invert the Laplace transformation. The function $lp(r, r_p, v_p)$ can be found by making the connection

$$lp(r, r_p, v_p) \Leftrightarrow |v_p| lp(r, r_p, v_p^2). \quad (\text{B9})$$

The final result is

$$\begin{aligned} lp(r, r_p, v_p) &= \frac{1}{\sqrt{2\pi}} \frac{\Gamma(\alpha+1)}{\Gamma(\alpha+\frac{1}{2})} \frac{(r/c)^{2\beta}}{(1+(r/c)^2)^{\beta+\gamma}} \times \\ &\psi(r)^{\alpha-1/2} \sum_{j=0}^{\infty} (\beta+\gamma)_j \frac{\xi^j}{j!} (\sin \eta)^{2j} \times \\ &\sum_{i=0}^{\infty} \binom{1}{2}_{i+j} \frac{(-\beta)_i}{(i+j)!} \left(1 - \frac{v_p^2}{2\psi(r)}\right)^{-(i+j)+\alpha-1/2} \times \\ &\frac{(\sin \eta)^{2i}}{i!} {}_2F_1(-i+j, \alpha; \frac{1}{2}; \frac{v_p^2}{2\psi(r)}). \end{aligned} \quad (\text{B10})$$

This formal result contains two infinite sums that diverge when implemented. Only when β is a positive integer and $\beta + \gamma$ is a negative integer do both sums terminate after a finite number of terms.

APPENDIX C: ERROR ANALYSIS ON THE COEFFICIENTS

The minimisation problem is a least squares problem with constraints. The r active constraints can be dealt with by the introduction of r Lagrange multipliers that form a vector \mathbf{d} . The function that has to be minimised is

$$\chi^2 = \mathbf{c}^t \mathbf{D} \mathbf{c} - 2\mathbf{p}^t \mathbf{c} + e + 2\mathbf{d}^t (\mathbf{A} \mathbf{c} - \mathbf{b}). \quad (\text{C1})$$

Here the element A_{is} of the matrix \mathbf{A} is the value of the DF of the i -th component on the s -th grid-point in phase

space, where the DF may reach its lower boundary b^s , which is usually zero. Standard theory leads to the m so-called normal equations

$$\mathbf{D} \mathbf{c} + \mathbf{A}^t \mathbf{d} = \mathbf{p} \quad (\text{C2})$$

that have to be solved, along with the r active constraints

$$\mathbf{A} \mathbf{c} = \mathbf{b}, \quad (\text{C3})$$

for the $m+r$ unknowns \mathbf{c} and \mathbf{d} . One obtains the system

$$\mathbf{M} \begin{pmatrix} \mathbf{c} \\ \mathbf{d} \end{pmatrix} = \begin{pmatrix} \mathbf{D} & \mathbf{A}^t \\ \mathbf{A} & \mathbf{0} \end{pmatrix} \begin{pmatrix} \mathbf{c} \\ \mathbf{d} \end{pmatrix} = \begin{pmatrix} \mathbf{p} \\ \mathbf{b} \end{pmatrix}. \quad (\text{C4})$$

This can be solved for the coefficients c_i

$$\begin{aligned} c_i &= M_{ij}^{-1} p^j + M_{is}^{-1} b^s \\ &= M_{ij}^{-1} g_n^j g_n w^n + M_{is}^{-1} b^s \\ &= F_i^n g_n + M_{is}^{-1} b^s. \end{aligned} \quad (\text{C5})$$

Here i and j range from 1 to m and s varies between 1 and r . The coefficients are written as a linear combination of the data points with the aid of the matrix $F_i^n = w^n M_{ij}^{-1} g_n^j$ (no summation over n), where $n = 1, \dots, N$, which is independent of the data points g_n . The covariance matrix of the coefficients, $\Sigma_{ij}(c)$, can be found using

$$\begin{aligned} \Sigma_{ij}(c) &= \langle (c_i - \bar{c}_i)(c_j - \bar{c}_j) \rangle \\ &= F_i^n F_j^m \langle (g_n - \bar{g}_n)(g_m - \bar{g}_m) \rangle \\ &= F_i^n \Sigma_{nm}(g) F_j^m. \end{aligned} \quad (\text{C6})$$

The covariance matrix of the data points is approximated by $\Sigma_{nm}(g) = \delta_{nm}/w^n$. Inserting the explicit form of the elements of \mathbf{F} one finds

$$\Sigma_{ij}(c) = M_{il}^{-1} D^{kl} M_{jk}^{-1}. \quad (\text{C7})$$

In the absence of positivity constraints on the DF ($\mathbf{A} = \mathbf{0}$) the covariance matrix of the coefficients is simply the inverse of the Hessian matrix. Taking the constraints into account

is expected to decrease the width of the errorbars since the positivity constraint rejects a lot of otherwise acceptable (but unphysical) fits to the data.

Knowing the error on the coefficients it is also possible to obtain errorbars on every function that depends on these coefficients

$$\sigma(f(c_1, \dots, c_m)) \approx \sqrt{\frac{\partial f}{\partial c_i} \Sigma_{ij}(c) \frac{\partial f}{\partial c_j}}. \quad (\text{C8})$$

For instance, the error on a LOSVD of the fitted model becomes

$$\sigma(\phi(v_p, x_p, y_p)) = \sqrt{\phi^i(v_p, x_p, y_p) \Sigma_{ij}(c) \phi^j(v_p, x_p, y_p)}. \quad (\text{C9})$$

The elements of the Hessian matrix scale approximately proportional to the square of the signal to noise ratio. This means that the error on the coefficients, neglecting the influence of the positivity constraints, scales inversely proportional to the signal to noise ratio.

The Hessian matrix is also influenced by the fact whether or not the components are linearly independent. When two components are linearly dependent, their coefficients can have an infinity of values without changing the outcome of the fit, balancing the one component with the other. The errorbars on the derived quantities, e.g. the LOSVDs, do not take into account this balancing and just measure the extreme values of these quantities, given the extreme values of the coefficients. Consequently, the errorbars will be infinitely large when linearly dependent components are used. This is reflected by the Hessian matrix being singular, rendering its inversion impossible. When nearly linearly dependent components are used, the Hessian will be close to singular, resulting in large errorbars.

REFERENCES

- Bender, R., 1990, *A&A*, 229,441
 Dejonghe, H., 1986, *Physics Reports*, 133
 Dejonghe, H., 1987, *MNRAS*, 224, 13
 Dejonghe, H., 1989, *ApJ*, 343, 113
 Dejonghe, H. & Merritt, D., 1992, *ApJ*, 391,531
 Franx, M., Illingworth, G. D., Heckman, T., 1989, *ApJ*, 327, 613
 Gerhard, O. E., 1993, *MNRAS*, 265, 213
 Gerhard, O. E., Jeske, G., Saglia, R. P. & Bender, R., 1998, *MNRAS*, 295, 702
 Kuijken K. & Merrifield, M. R., 1993, 264, 712
 Merritt, D. & Oh, S. P., 1996, *AJ*, 113, 1279
 Rix, H. W. & White, S. D. M., 1992, *MNRAS*, 254, 389
 Rix, H. W., de Zeeuw, P. T., Carollo, C. M., Cretton, N. & van der Marel, R. P., *ApJ*, 488, 702
 Saha, P. & Williams, T. B., 1994, *AJ*, 107, 1295
 Sargent, W. L. W., Schechter, P. L., Boksenberg, A. & Shortridge, K., 1977, *ApJ*, 212, 326
 Simkin, S. M., 1974, *A&A*, 31, 129
 Statler, T. S., 1991, *AJ*, 102, 882
 Tonry, J. L. & Davis, M., 1979, *AJ*, 84, 1511
 van der Marel, R. P. & Franx, M., 1993, *ApJ*, 407, 525
 Winsall, M., 1991, unpublished, PhD. thesis